Engineering and Technology
2015; 2(5): 312-323
Published online July 10, 2015 (http://www.aascit.org/journal/et)

AASCIT American Association for Science and Technology

Keywords
Wilcox and Rubesin Model,
Wilcox Model,
Jacon and Knight Model,
Zhou *et al.* Model,
Navier-Stokes Equations

Received: June 7, 2015
Revised: June 19, 2015
Accepted: June 20, 2015

Comparison of Several Turbulence Models as Applied to Hypersonic Flows in 2D

Edisson S. G. Maciel

Aeronautical Engineering Division (IEA), Aeronautical Technological Institute (ITA), São José dos Campos, SP, Brasil

Email address
edisavio@edissonsavio.eng.br

Citation
Edisson S. G. Maciel. Comparison of Several Turbulence Models as Applied to Hypersonic Flows in 2D. *Engineering and Technology.* Vol. 2, No. 5, 2015, pp. 312-323.

Abstract
In the present work, the Van Leer flux vector splitting scheme is implemented to solve the two-dimensional Favre-averaged Navier-Stokes equations. The Wilcox and Rubesin, Wilcox, Jacon and Knight, and Zhou, Davidson and Olsson two-equation models are used in order to close the problem. The physical problem under study is the "cold gas" hypersonic flow around a reentry capsule configuration. The results have demonstrated that the aerodynamic coefficient of lift is better predicted by the Wilcox and Rubesin turbulence model; However, the stagnation pressure ahead of the reentry capsule configuration is better predicted by the Wilcox turbulence model.

1. Introduction

Conventional non-upwind algorithms have been used extensively to solve a wide variety of problems ([1]). Conventional algorithms are somewhat unreliable in the sense that for every different problem (and sometimes, every different case in the same class of problems) artificial dissipation terms must be specially tuned and judicially chosen for convergence. Also, complex problems with shocks and steep compression and expansion gradients may defy solution altogether.

First order upwind schemes are in general more robust but are also more involved in their derivation and application. Some upwind schemes that have been applied to the Euler equations are, for example, [2-3]. Some comments about these methods are reported below:

[2] suggested an upwind scheme based on the flux vector splitting concept. This scheme considered the fact that the convective flux vector components could be written as flow Mach number polynomial functions, as main characteristic. Such polynomials presented the particularity of having the minor possible degree and the scheme had to satisfy seven basic properties to form such polynomials. This scheme was presented to the Euler equations in Cartesian coordinates and three-dimensions.

[3] emphasized that the [4] scheme had low computational complexity and low numerical diffusion when compared to other methods. They also mentioned that the original method had several deficiencies. It yielded pressure oscillations in the proximity of shock waves. Problems with adverse mesh and with flow alignment were also reported. [3] proposed a hybrid flux vector splitting approach which alternated between the [4] scheme and the [2] scheme, at the shock-wave regions. This strategy assured that strength shock resolution was clearly and well defined.

There is a practical necessity in the aeronautical industry and in other fields of the capability of calculating separated turbulent compressible flows. With the available numerical methods, researches seem able to analyze several separated flows, three-dimensional in general, if an appropriated turbulence model is employed. Simple methods as the algebraic turbulence models of [5-6] supply satisfactory results with low computational cost and allow that the main features of the turbulent flow be detected.

Several studies concerning two-equation models have been developed by the CFD ("Computational Fluid Dynamics") community. [7] have programmed a k-ω^2 turbulence model that used the definition of the turbulent Reynolds number and a damping factor to define the turbulent viscosity. [8] has presented a more compact and elegant form of the k-ω two-equation model, popularized until now. [9] have developed an unstructured algorithm to solve the Reynolds-averaged Navier-Stokes equations in two-dimensions. The turbulence effects were modeled with the standard k-ε model of [8]. [10] have defined a viscous and temperature lengths to construct a variable Prandtl number.

This work describes four turbulence models applied to hypersonic flows in two-dimensions. The [2] scheme, in its first-order version, is implemented to accomplish the numerical simulations. The Favre-averaged Navier-Stokes equations, on a finite volume context and employing structured spatial discretization, are applied to solve the "cold gas" hypersonic flow around a reentry capsule in two-dimensions. Turbulence models are applied to close the system, namely: [7-10]. The convergence process is accelerated to the steady state condition through a spatially variable time step procedure, which has proved effective gains in terms of computational acceleration (see [11-12]). The results have shown that the [7] scheme yields the best results in terms of the prediction of the lift aerodynamic coefficient; however, the [8] turbulence model predicts the best value of the stagnation pressure. Moreover, the [8] scheme also predicted the most severe pressure field.

2. Navier-Stokes Equations

The two-dimensional flow is modeled by the Navier-Stokes equations, which express the conservation of mass and energy as well as the momentum variation of a viscous, heat conducting and compressible media, in the absence of external forces. The Navier-Stokes equations are presented in their two-equation turbulence model formulation. The integral form of these equations may be represented by:

$$\partial/\partial t\int_V Q dV+\int_S\left[(E_e-E_v)n_x+(F_e-F_v)n_y\right]dS+\int_V G dV=0\,,\quad(1)$$

where Q is written for a Cartesian system, V is the cell volume, n_x and n_y are components of the unity vector normal to the cell boundary, S is the flux area, E_e and F_e are the components of the convective, or Euler, flux vector, E_v and F_v are the components of the viscous, or diffusive, flux vector and G is the source term of the two-equation models. The vectors Q, E_e, F_e, E_v and F_v are, incorporating a k-s formulation, represented by:

$$Q=\begin{Bmatrix}\rho\\ \rho u\\ \rho v\\ e\\ \rho k\\ \rho s\end{Bmatrix},\ E_e=\begin{Bmatrix}\rho u\\ \rho u^2+p\\ \rho uv\\ (e+p)u\\ \rho ku\\ \rho su\end{Bmatrix},\ F_e=\begin{Bmatrix}\rho v\\ \rho uv\\ \rho v^2+p\\ (e+p)v\\ \rho kv\\ \rho sv\end{Bmatrix},\ E_v=\begin{Bmatrix}0\\ t_{xx}+\tau_{xx}\\ t_{xy}+\tau_{xy}\\ f_x\\ \alpha_x\\ \beta_x\end{Bmatrix},\ F_v=\begin{Bmatrix}0\\ t_{xy}+\tau_{xy}\\ t_{yy}+\tau_{yy}\\ f_y\\ \alpha_y\\ \beta_y\end{Bmatrix},\ \text{and } G=\begin{Bmatrix}0\\ 0\\ 0\\ 0\\ G_k\\ G_s\end{Bmatrix},\quad(2)$$

where the components of the viscous stress tensor are defined as:

$$t_{xx}=\left[2\mu_M\,\partial u/\partial x-2/3\,\mu_M\left(\partial u/\partial x+\partial v/\partial y\right)\right]/Re\ ;\quad(3a)$$

$$t_{xy}=\mu_M\left(\partial u/\partial y+\partial v/\partial x\right)/Re\,;$$

$$t_{yy}=\left[2\mu_M\left(\partial v/\partial y\right)-2/3\,\mu_M\left(\partial u/\partial x+\partial v/\partial y\right)\right]/Re\ .\quad(3b)$$

The components of the turbulent stress tensor (Reynolds stress tensor) are described by the following expressions:

$$\begin{aligned}\tau_{xx}&=\left[2\mu_T\,\partial u/\partial x-2/3\,\mu_T\left(\partial u/\partial x+\partial v/\partial y\right)\right]/Re-2/3\,\rho k;\\ \tau_{xy}&=\mu_T\left(\partial u/\partial y+\partial v/\partial x\right)/Re;\\ \tau_{yy}&=\left[2\mu_T\,\partial v/\partial y-2/3\,\mu_T\left(\partial u/\partial x+\partial v/\partial y\right)\right]/Re-2/3\,\rho k.\end{aligned}\quad(4)$$

Expressions to f_x and f_y are given bellow:

$$\begin{aligned}f_x&=\left(t_{xx}+\tau_{xx}\right)u+\left(t_{xy}+\tau_{xy}\right)v-q_x,\\ f_y&=\left(t_{xy}+\tau_{xy}\right)u+\left(t_{yy}+\tau_{yy}\right)v-q_y,\end{aligned}\quad(5)$$

where q_x and q_y are the Fourier heat flux components and are given by:

$$\begin{aligned}q_x&=-\gamma/Re\left(\mu_M/Pr_L+\mu_T/Pr_T\right)\partial e_i/\partial x,\\ q_y&=-\gamma/Re\left(\mu_M/Pr_L+\mu_T/Pr_T\right)\partial e_i/\partial y.\end{aligned}\quad(6)$$

The diffusion terms related to the k-s equations are given by:

$$\begin{aligned}\alpha_x&=1/Re\left(\mu_M+\mu_T/\sigma_k\right)\partial k/\partial x,\\ \alpha_y&=1/Re\left(\mu_M+\mu_T/\sigma_k\right)\partial k/\partial y;\end{aligned}\quad(7)$$

$$\beta_x = 1/\mathrm{Re}(\mu_M + \mu_T/\sigma_s)\partial s/\partial x,$$
$$\beta_y = 1/\mathrm{Re}(\mu_M + \mu_T/\sigma_s)\partial s/\partial y. \tag{8}$$

In the above equations, ρ is the fluid density; u and v are Cartesian components of the velocity vector in the x and y directions, respectively; e is the total energy per unit volume; p is the static pressure; k is the turbulence kinetic energy; s is the second turbulent variable, which is the rate of dissipation of the turbulence kinetic energy (k-ε model), the turbulent vorticity (k-ω model) or the square of the turbulent vorticity (k-ω^2 model); the t's are viscous stress components; τ's are the Reynolds stress components; the q's are the Fourier heat flux components; G_k takes into account the production and the dissipation terms of k; G_s takes into account the production and the dissipation terms of s; μ_M and μ_T are the molecular and the turbulent viscosities, respectively; Pr_L and Pr_T are the laminar and the turbulent Prandtl numbers, respectively; σ_k and σ_s are turbulence coefficients; γ is the ratio of specific heats; Re is the laminar Reynolds number, defined by:

$$\mathrm{Re} = \rho V_{REF} l_{REF}/\mu_M, \tag{9}$$

where V_{REF} is a characteristic flow velocity and l_{REF} is a configuration characteristic length. The internal energy of the fluid, e_i, is defined as:

$$e_i = e/\rho - 0.5(u^2 + v^2). \tag{10}$$

The molecular viscosity is estimated by the empiric Sutherland formula:

$$\mu_M = bT^{1/2}/(1 + S/T), \tag{11}$$

where T is the absolute temperature (K), b = 1.458x10^{-6} Kg/(m.s.$K^{1/2}$) and S = 110.4 K, to the atmospheric air in the standard atmospheric conditions ([13]).

The Navier-Stokes equations are dimensionless in relation to the freestream density, ρ_∞, the freestream speed of sound, a_∞, and the freestream molecular viscosity, μ_∞. The system is closed by the state equation for a perfect gas:

$$p = (\gamma - 1)\left[e - 0.5\rho(u^2 + v^2) - \rho k\right], \tag{12}$$

considering the ideal gas hypothesis. The total enthalpy is given by $H = (e + p)/\rho$.

3. Van Leer Algorithm

The space approximation of the integral Equation (1) yields an ordinary differential equation system given by:

$$V_{i,j}\, dQ_{i,j}/dt = -R_{i,j}, \tag{13}$$

with $R_{i,j}$ representing the net flux (residual) of the conservation of mass, conservation of momentum and conservation of energy in the volume $V_{i,j}$. The residual is calculated as:

$$R_{i,j} = R_{i,j-1/2} + R_{i+1/2,j} + R_{i,j+1/2} + R_{i-1/2,j}, \tag{14}$$

with $R_{i+1/2,j} = R^c_{i+1/2,j} - R^d_{i+1/2,j}$, where the superscripts "c" and "d" are related to convective and diffusive contributions, respectively. The cell volume is given by:

$$V_{i,j} = 0.5\left|(x_{i,j} - x_{i+1,j})y_{i+1,j+1} + (x_{i+1,j} - x_{i+1,j+1})y_{i,j} + (x_{i+1,j+1} - x_{i,j})y_{i+1,j}\right| + 0.5\left|(x_{i,j} - x_{i+1,j+1})y_{i,j+1} + (x_{i+1,j+1} - x_{i,j+1})y_{i,j} + (x_{i,j+1} - x_{i,j})y_{i+1,j+1}\right|. \tag{15}$$

The convective discrete flux calculated by the AUSM scheme (Advection Upstream Splitting Method) can be understood as a sum of the arithmetical average between the right (R) and left (L) states of the cell face (i+½,j), involving volumes (i+1,j) and (i,j), respectively, multiplied by the interface Mach number, plus a scalar dissipative term, as shown in [4]. Hence,

$$R_{i+1/2,j} = |S|_{i+1/2,j}\left\{\frac{1}{2}M_{i+1/2,j}\left(\begin{bmatrix}\rho a\\ \rho au\\ \rho av\\ \rho aH\\ \rho ak\\ \rho as\end{bmatrix}_L + \begin{bmatrix}\rho a\\ \rho au\\ \rho av\\ \rho aH\\ \rho ak\\ \rho as\end{bmatrix}_R\right) - \frac{1}{2}\varphi_{i+1/2,j}\left(\begin{bmatrix}\rho a\\ \rho au\\ \rho av\\ \rho aH\\ \rho ak\\ \rho as\end{bmatrix}_R - \begin{bmatrix}\rho a\\ \rho au\\ \rho av\\ \rho aH\\ \rho ak\\ \rho as\end{bmatrix}_L\right)\right\} + \begin{bmatrix}0\\ S_x p\\ S_y p\\ 0\\ 0\\ 0\end{bmatrix}_{i+1/2,j}, \tag{16}$$

where $S_{i+1/2,j} = \begin{bmatrix}S_x & S_y\end{bmatrix}^t_{i+1/2,j}$ defines the normal area vector for the surface (i+½,j). The normal area components S_x and S_y to each flux interface are given in Tab. 1. Figure 1 exhibits the computational cell adopted for the simulations, as well its respective nodes and flux interfaces.

Table 1. *Values of S_x and S_y.*

Surface	S_x	S_y
i,j-1/2	$(y_{i+1,j} - y_{i,j})$	$(x_{i,j} - x_{i+1,j})$
i+1/2,j	$(y_{i+1,j+1} - y_{i+1,j})$	$(x_{i+1,j} - x_{i+1,j+1})$
i,j+1/2	$(y_{i,j+1} - y_{i+1,j+1})$	$(x_{i+1,j+1} - x_{i,j+1})$
i-1/2,j	$(y_{i,j} - y_{i,j+1})$	$(x_{i,j+1} - x_{i,j})$

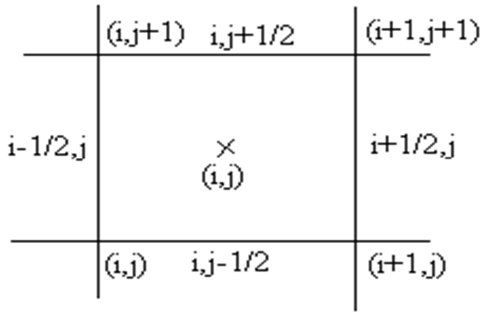

Figure 1. *Computational Cell.*

The quantity "a" represents the speed of sound, which is defined as:

$$a = (\gamma p/\rho - k)^{0.5}. \tag{17}$$

$M_{i+½,j}$ defines the advective Mach number at the (i+½,j) face, which is calculated according to [4]:

$$M_{i+1/2,j} = M_L^{+} + M_R^{-}, \tag{18}$$

where the separated Mach numbers are defined by [2]:

$$M^{+} = \begin{bmatrix} M, & \text{if } M \geq 1; \\ 0.25(M+1)^2, & \text{if } |M| < 1; \\ 0, & \text{if } M \leq -1; \end{bmatrix} \quad \text{and} \quad M^{-} = \begin{bmatrix} 0, & \text{if } M \geq 1; \\ -0.25(M-1)^2, & \text{if } |M| < 1; \\ M, & \text{if } M \leq -1. \end{bmatrix} \tag{19}$$

M_L and M_R represent the Mach numbers associated with the left and the right states, respectively. The advection Mach number is defined by:

$$M = (S_x u + S_y v)/(a|S|). \tag{20}$$

The pressure at the face (i+½,j), related to the cell (i,j), is calculated by a similar formula:

$$p_{i+1/2,j} = p_L^{+} + p_R^{-}, \tag{21}$$

with $p^{+/-}$ denoting the pressure separation and due to [2]:

$$p^{+} = \begin{bmatrix} p, & \text{if } M \geq 1; \\ 0.25p(M+1)^2(2-M), & \text{if } |M| < 1; \\ 0, & \text{if } M \leq -1; \end{bmatrix} \quad \text{and} \quad p^{-} = \begin{bmatrix} 0, & \text{if } M \geq 1; \\ 0.25p(M-1)^2(2+M), & \text{if } |M| < 1; \\ p, & \text{if } M \leq -1. \end{bmatrix} \tag{22}$$

The definition of a dissipative term ϕ determines the particular formulation of the convective fluxes. The following choice corresponds to the [2] scheme, according to [3]:

$$\phi_{i+1/2,j} = \phi_{i+1/2,j}^{VL} = \begin{cases} |M_{i+1/2,j}|, & \text{if } |M_{i+1/2,j}| \geq 1; \\ |M_{i+1/2,j}| + 0.5(M_R - 1)^2, & \text{if } 0 \leq M_{i+1/2,j} < 1; \\ |M_{i+1/2,j}| + 0.5(M_L + 1)^2, & \text{if } -1 < M_{i+1/2,j} \leq 0. \end{cases} \tag{23}$$

The above equations clearly show that to a supersonic cell face Mach number, the [2] scheme represents a discretization purely upwind, using either the left state or the right state to the convective terms and to the pressure, depending of the Mach number signal. This [2] scheme is first order accurate in space. The time integration is performed using an explicit Runge-Kutta method of five stages, second order accurate, and can be represented in generalized form by:

$$\begin{aligned} Q_{i,j}^{(0)} &= Q_{i,j}^{(n)} \\ Q_{i,j}^{(k)} &= Q_{i,j}^{(0)} - \alpha_k \Delta t_{i,j}\left[R\left(Q_{i,j}^{(k-1)}\right)/V_{i,j} + G\left(Q_{i,j}^{(k-1)}\right)\right], \\ Q_{i,j}^{(n+1)} &= Q_{i,j}^{(k)} \end{aligned} \tag{24}$$

with k = 1,...,5; $\alpha_1 = 1/4$, $\alpha_2 = 1/6$, $\alpha_3 = 3/8$, $\alpha_4 = 1/2$ and $\alpha_5 = 1$. The gradients of the primitive variables are calculated using the Green theorem, which considers that the gradient of a primitive variable is constant at the volume and that the volume integral which defines the gradient is replaced by a surface integral ([14]). To the $\partial u/\partial x$ gradient, for example, it is possible to write:

$$\frac{\partial u}{\partial x} = \frac{1}{V}\int_V \frac{\partial u}{\partial x} dV = \frac{1}{V}\int_S u\left(\vec{n}_x \bullet d\vec{S}\right) = \frac{1}{V}\int_{S_x} u dS_x \cong \tag{25a}$$

$$\frac{1}{V}\left[0.5\left(u_{i,j} + u_{i,j-1}\right)S_{x_{i,j-1/2}} + 0.5\left(u_{i,j} + u_{i+1,j}\right)S_{x_{i+1/2,j}} + 0.5\left(u_{i,j} + u_{i,j+1}\right)S_{x_{i,j+1/2}} + 0.5\left(u_{i,j} + u_{i-1,j}\right)S_{x_{i-1/2,j}}\right]. \tag{25b}$$

4. Turbulence Models

4.1. Wilcox and Rubesin Turbulence Model

In the [7] turbulence model, s = ω^2. To define the turbulent viscosity, or eddy viscosity, it is necessary to define the turbulent Reynolds number:

$$\mathrm{Re}_T = k/(\nu_M \omega), \quad \text{with: } \nu_M = \mu_M/\rho. \tag{26}$$

It is also necessary to determine the D damping factor:

$$D = 1 - \alpha e^{[-\mathrm{Re}_T]}. \tag{27}$$

The turbulent viscosity is expressed in terms of k and ω as:

$$\mu_T = \mathrm{Re}\, D\rho k/\omega. \tag{28}$$

The source term denoted by G in the governing equation contains the production and dissipation terms of k and ω^2. To the [7] model, the G_k and G_{ω^2} terms have the following expressions:

$$G_k = -P_k - D_k \quad \text{and} \quad G_{\omega^2} = -P_{\omega^2} - D_{\omega^2}, \tag{29}$$

where:

$$P = \left(\frac{\partial u}{\partial y} + \frac{\partial v}{\partial x}\right)\frac{\partial u}{\partial y}, P_k = \left(\frac{DP}{\omega^2}\right)\rho\omega k \Big/ \mathrm{Re}; D_k = \left[-\frac{2}{3}\left(\frac{\partial u}{\partial x} + \frac{\partial v}{\partial y}\right)\Big/\omega - \beta^*\right]\rho\omega k \Big/ \mathrm{Re}; \tag{30}$$

$$P_{\omega^2} = \left(\frac{\gamma_\infty EP}{\omega^2}\right)\rho\omega^3 \Big/ \mathrm{Re}; D_{\omega^2} = \left[-\frac{2}{3}\gamma_\infty\left(\frac{\partial u}{\partial x} + \frac{\partial v}{\partial y}\right)\Big/\omega - \left(\beta + \frac{2}{\sigma_{\omega^2}}\right)\left(\frac{d\sqrt{k/\omega}}{dy}\right)^2\right]\rho\omega^3 \Big/ \mathrm{Re}, \tag{31}$$

with the second damping factor E defined as: $E = 1 - \alpha e^{(-0.5\mathrm{Re}_T)}$. The closure coefficients adopted for the [7] model assume the following values: $\sigma_k = 2.0$; $\sigma_{\omega^2} = 2.0$; $\beta^* = 0.09$; $\beta = 0.15$; $\alpha = 0.99174$; $\gamma_\infty = 0.9$; Prd_L = 0.72; Prd_T = 0.9.

4.2. Wilcox Turbulence Model

In the [8] turbulence model, s = ω. The turbulent viscosity is expressed in terms of k and ω as:

$$\mu_T = \mathrm{Re}\,\rho k/\omega. \tag{32}$$

In this model, the quantities σ_k and σ_ω have the values $1/\sigma^*$ and $1/\sigma$, respectively, where σ^* and σ are model constants. To the [8] model, the G_k and G_ω terms have the following expressions:

$$G_k = -P_k + D_k \quad \text{and} \quad G_\omega = -P_\omega + D_\omega, \tag{33}$$

where:

$$P_k = \mu_T\left(\frac{\partial u}{\partial y} + \frac{\partial v}{\partial x}\right)\frac{\partial u}{\partial y}\Big/\mathrm{Re} \quad \text{and} \quad D_k = \beta^*\rho k\,\omega/\mathrm{Re};$$

$$P_\omega = \left(\frac{\alpha\omega}{k}\right)P_k \quad \text{and} \quad D_\omega = \beta\rho\,\omega^2/\mathrm{Re}, \tag{34}$$

where the closure coefficients adopted for the [8] model are: $\beta^* = 0.09$; $\beta = 3/40$; $\sigma^* = 0.5$; $\sigma = 0.5$; $\alpha = 5/9$; Prd_L = 0.72; Prd_T = 0.9.

4.3. Jacon and Knight Turbulence Model

In the [9] turbulence model, it is necessary to define the dissipation rate, which is decomposed as follows:

$$\varepsilon = \varepsilon_s + \varepsilon_d, \tag{35}$$

where ε_d is the dissipation of the dilatation of the turbulent kinetic energy. The Sarkar model is employed to take into account the compressibility effects:

$$\varepsilon_d = M_t^2\varepsilon_s \quad \text{and} \quad M_t^2 = 2k/a^2, \tag{36}$$

with M_t being the turbulent Mach number. The turbulent viscosity is expressed in terms of k and ε as:

$$\mu_T = \mathrm{Re}\, C_\mu\,\rho k^2/\varepsilon. \tag{37}$$

The source term denoted by G in the flow equations has the production and dissipation terms of k and ε. To the model of [9], the terms G_k and G_ε have the following expressions:

$$G_k = P_k + D_k \quad \text{and} \quad G_\varepsilon = P_\varepsilon + D_\varepsilon, \tag{38}$$

where:

$$\begin{aligned} &P_k = -\tau_{xx}\,\partial u/\partial x - \tau_{xy}\left(\partial u/\partial y + \partial v/\partial x\right) - \tau_{yy}\,\partial v/\partial y; D_k = \rho\varepsilon; \\ &P_\varepsilon = C_{\varepsilon1}P_k\,\varepsilon/k; D_\varepsilon = C_{\varepsilon2}\rho\varepsilon_s^2/k. \end{aligned} \tag{39}$$

The closure coefficients of the [9] model assume the following values: $C_{\varepsilon1} = 1.44$, $C_{\varepsilon2} = 1.92$, $C_\mu = 0.09$, $\sigma_k = 1.0$, $\sigma_\varepsilon = 1.3$, $Pr_L = 0.72$ and $Pr_T = 0.89$.

4.4. Zhou, Davidson and Olsson Turbulence Model

To the [10] turbulence model, s = ε. Before define the turbulent viscosity, it is necessary to define some parameters. The coefficient C_l is defined as

$$C_l = \kappa C_\mu^{-0.75} . \quad (40)$$

The characteristic viscous length is expressed as

$$l_\mu = C_l N\left[1 - e^{-\sqrt{k}N/(A_\mu \nu_m)}\right], \quad (41)$$

where N is the normal distance of a cell from the wall. The turbulent viscosity is defined as

$$\mu_T = \mathrm{Re}\, C_\mu \rho \sqrt{k}\, l_\mu . \quad (42)$$

The characteristic temperature length is expressed as

$$l_t = C_3 N\left[1 - e^{-\sqrt{k}N/(C_4 \nu_m)}\right]. \quad (43)$$

The variable turbulent Prandtl number, to be inserted in Eq. (6), is defined as

$$Pr_{T,var} = l_\mu / l_t . \quad (44)$$

The G_k and G_ε terms have the following expressions:

$$G_k = -P_k + D_k \quad \text{and} \quad G_\varepsilon = -P_\varepsilon + D_\varepsilon , \quad (45)$$

where:

$$\tau_{xy} = \mu_T\left(\frac{\partial u}{\partial y} + \frac{\partial v}{\partial x}\right)\Big/\mathrm{Re},\ P_k = \tau_{xy}\frac{\partial u}{\partial y};\ D_k = \rho\varepsilon/\mathrm{Re}; \quad (46)$$

$$P_\varepsilon = \frac{\varepsilon}{k}C_{1\varepsilon}P_k,\ D_\varepsilon = \frac{\varepsilon}{k}C_{2\varepsilon}\rho\varepsilon/\mathrm{Re}. \quad (47)$$

The closure coefficients assume the following values: $C_{1\varepsilon} = 1.44$, $C_{2\varepsilon} = 1.92$, $C_3 = 3.12$, $C_4 = 92.0$, $\kappa = 0.40$, $A_\mu = 70.0$, $C_\mu = 0.09$, $\sigma_k = 1.0$, $\sigma_\varepsilon = 1.3$ and $Pr_L = 0.72$.

5. Spatially Variable Time Step

The basic idea of this procedure consists in keeping a constant CFL number in all calculation domain; thus allowing that appropriated time steps to each specific mesh region could be used during the convergence process. Hence, to a viscous simulation and according to the [15] work, it is possible to write:

$$\Delta t_{i,j} = \left(\frac{CFL(\Delta t_c \Delta t_v)}{\Delta t_c + \Delta t_v}\right)_{i,j}, \quad (48)$$

with Δt_c being the convective time step and Δt_v being the viscous time step. These quantities are defined as:

$$\begin{aligned}
&(\Delta t_c)_{i,j} = \frac{V_{i,j}}{(\lambda_c)_{i,j}},\ (\lambda_c)_{i,j} = \max\left(\lambda^{max}_{i,j-1/2}, \lambda^{max}_{i+1/2,j}, \lambda^{max}_{i,j+1/2}, \lambda^{max}_{i-1/2,j}\right);\\
&\left(\lambda^{max}\right)_{int} = \left(\left|u_{int}n_x + v_{int}n_y\right| + a_{int}\right)S_{int},
\end{aligned} \quad (49)$$

$$\begin{aligned}
&(\Delta t_v)_{i,j} = K_v \frac{V_{i,j}}{(\lambda_v)_{i,j}},\ (p1)_{i,j} = \frac{\gamma^{3/2}M_\infty}{(\mathrm{Re}\,Pr\,d_L)V_{i,j}};\\
&(p2)_{i,j} = \frac{\mu_{i,j-1/2}}{\rho_{i,j-1/2}}S^2_{i,j-1/2} + \frac{\mu_{i+1/2,j}}{\rho_{i+1/2,j}}S^2_{i+1/2,j} + \frac{\mu_{i,j+1/2}}{\rho_{i,j+1/2}}S^2_{i,j+1/2} + \frac{\mu_{i-1/2,j}}{\rho_{i-1/2,j}}S^2_{i-1/2,j};\\
&(\lambda_v)_{i,j} = (p1 \times p2)_{i,j},
\end{aligned} \quad (50)$$

where interface properties are calculated by arithmetical average, M_∞ is the freestream Mach number, μ is the fluid molecular viscosity and K_v is equal to 0.25, as recommended by [15]. The initial and boundary conditions are reported in [16-17] and the interested reader is recommended to read these references to become aware of the numerical implementation.

6. Results

Tests were performed in a Dual Core processor of 2.3GHz and 2.0Gbytes of RAM microcomputer. Three orders of reduction of the maximum residual in the field were considered to obtain a converged solution. The residual was defined as the value of the discretized conservation equation. The entrance or attack angle was adopted equal to zero. The ratio of specific heats, γ, assumed the value 1.4.

Figure 2 shows the reentry capsule configuration. It is composed of 5,040 rectangular cells and 5,185 nodes, which is equivalent to a mesh of 85x61 nodes on a finite difference context. The exponential stretching is of 7.5%.

Detail of this mesh is shown in Fig. 3. The initial condition is defined in Tab. 2. The Reynolds number was estimated based on [13].

Table 2. *Initial Conditions.*

M_∞	θ	Altitude	L_∞	Re
7.0	0.0°	40,000m	3.0m	1.66×10^6

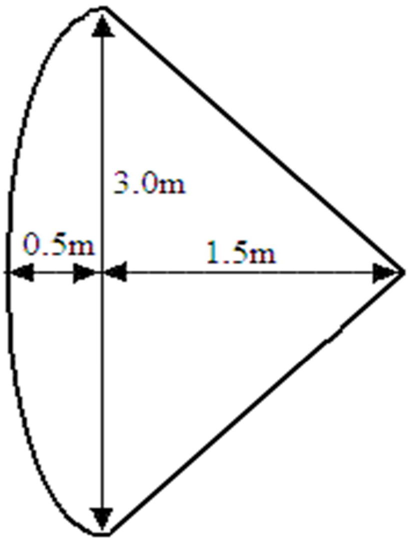

Figure 2. Reentry capsule configuration.

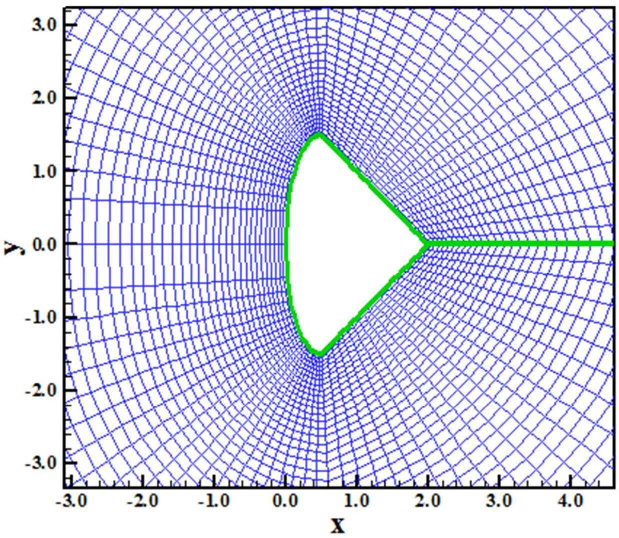

Figure 3. Reentry capsule viscous mesh.

6.1. Wilcox and Rubesin Results

Figure 4 exhibits the pressure contours obtained by the [2] scheme as using the [7] turbulence model. The shock is well captured and good symmetry properties are observed. The pressure peak reaches 43.62 unities. Figure 5 presents the Mach number contours obtained by the [2] scheme as using the [7] turbulence model. The Mach number contours are symmetrical and not pre-shock oscillations appear, as expected. The maximum Mach number value is 7.55, slightly superior to the freestream Mach number. Figure 6 shows the temperature contours obtained by the [2] scheme. The temperature field presents a maximum at the leading and at the trailing edge regions. The field presents good symmetry properties. The shock is well captured. The maximum temperature value reaches 2,772.12 K. Figure 7 exhibits the turbulent kinetic energy contours generated by the [2] scheme as using the [7] turbulence model. The plot presents good symmetry properties and the values of the turbulent kinetic energy are coherent.

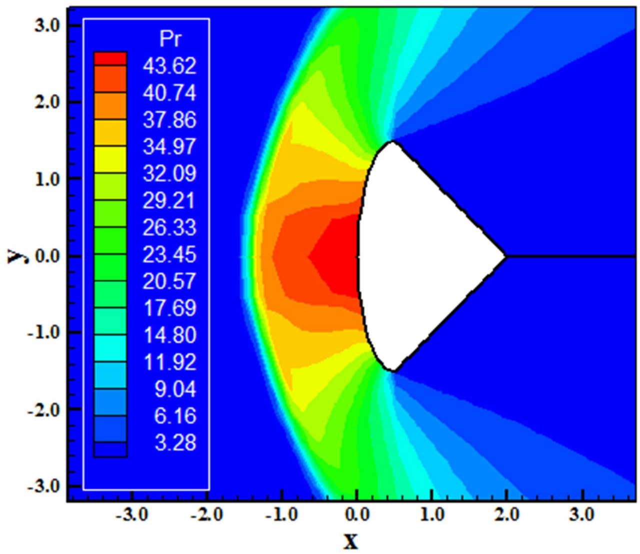

Figure 4. Pressure contours (WR).

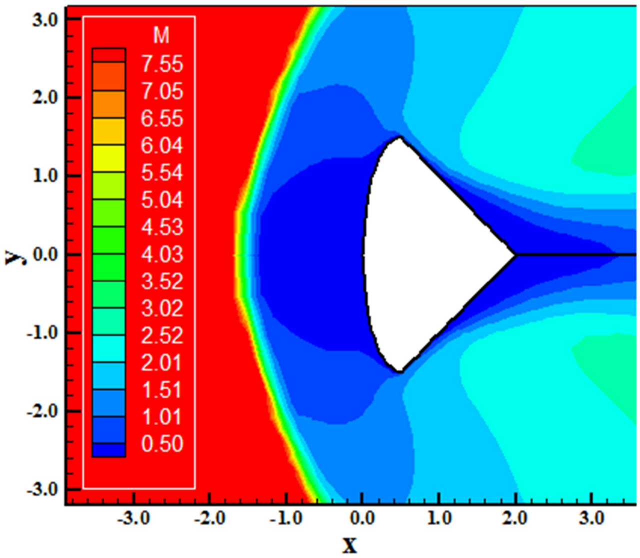

Figure 5. Mach number contours (WR).

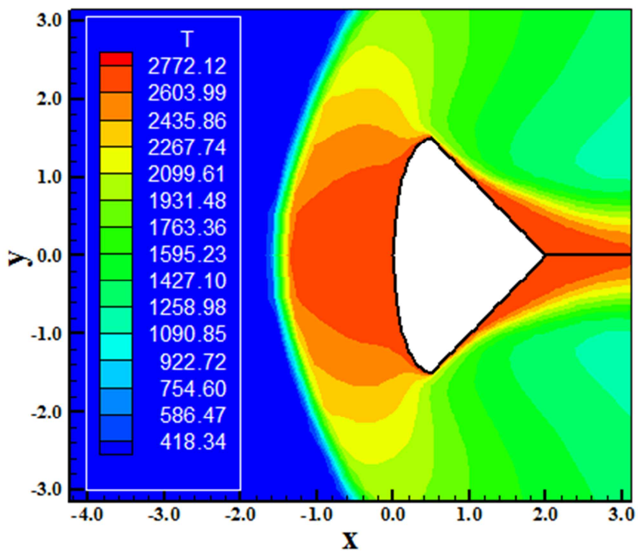

Figure 6. Temperature contours (WR).

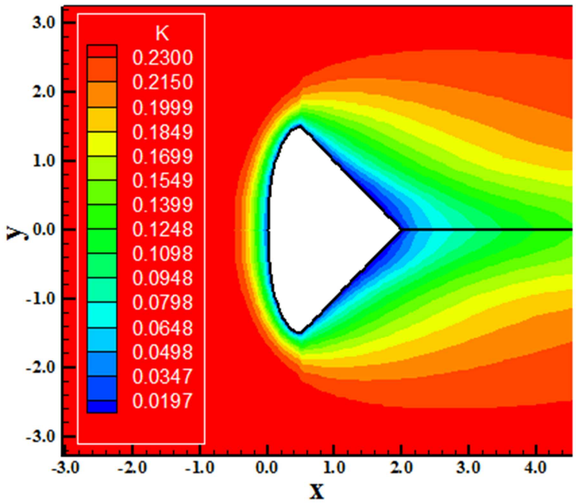

Figure 7. *Turbulent kinetic energy contours (WR).*

6.2. Wilcox Results

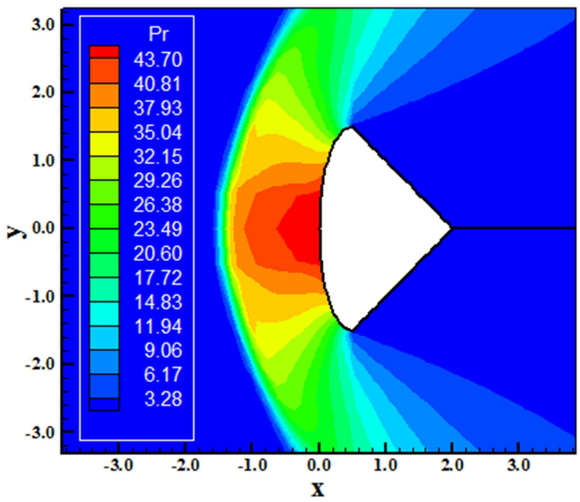

Figure 8. *Pressure contours (W).*

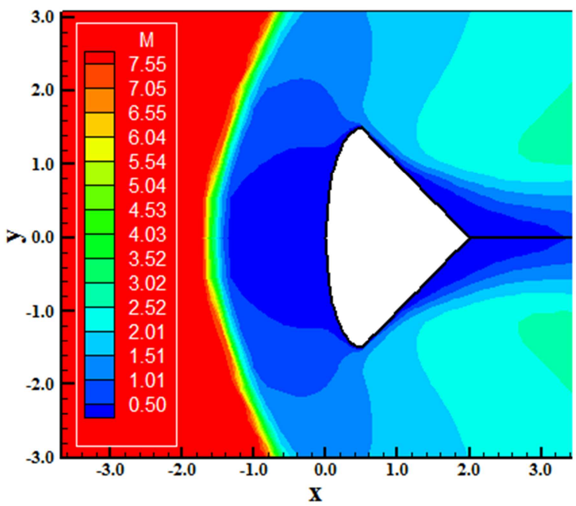

Figure 9. *Mach number contours (W).*

Figure 8 presents the pressure contours obtained by the [2] scheme as the [8] turbulence model is employed. The contours are symmetrical and homogeneous. No pre-shock oscillations are observed. The pressure peak is equal to 43.70 unities.

Figure 9 shows the Mach number contours obtained by the [2] scheme as using the [8] turbulence model. The Mach number peak is equal to 7.55, slightly superior to the freestream Mach number. The contours are symmetrical and homogeneous. The subsonic region is well captured at the leading edge region.

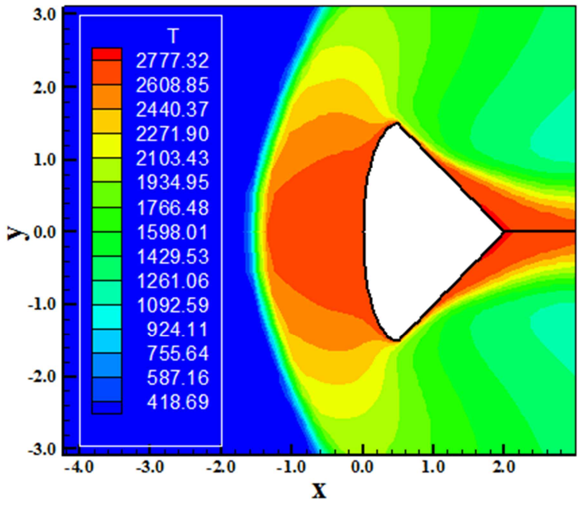

Figure 10. *Temperature contours (W).*

Figure 10 exhibits the temperature contours in the field obtained by the [2] scheme as using the [8] turbulence model. The temperature peak is close to 2,777.32 K and appears at the trailing edge. The contours are symmetrical and homogeneous. Figure 11 presents the turbulent kinetic energy contours obtained by the [2] scheme as using the [8] turbulence model. The contours are symmetrical, but differs from the same contours of the [7] turbulence model. This turbulent kinetic energy contours are more strength than the [7] ones.

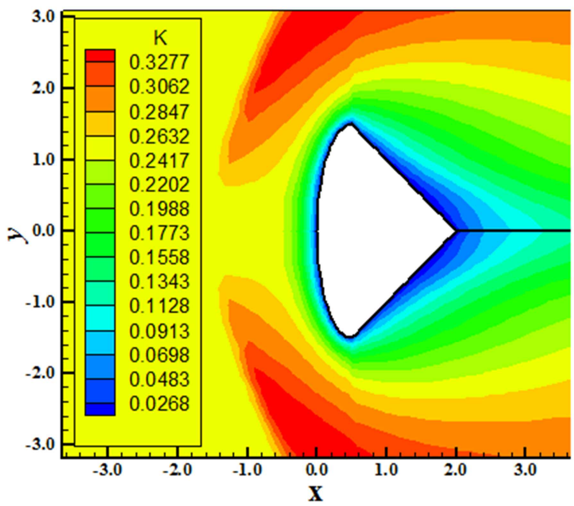

Figure 11. *Turbulent kinetic energy contours (W).*

6.3. Jacon and Knight Results

Figure 12 shows the pressure contours obtained by the [2] scheme as using the [9] turbulence model. As can be seen, the pressure contours are bad resolved. The contours are symmetrical, but the field seems not developed. The pressure peak is 3.97, well below the pressure peak of the [7] and [8] models. It seems that the k-ε model is very sensitive to the freestream Mach number, or, in other words, very sensitive to the hypersonic flow regime. Figure 13 exhibits the Mach number contours obtained by the [2] scheme as using the [9] turbulence model. The contours are again not developed. The Mach number peak is 6.97. The contours are symmetrical, but bad resolved.

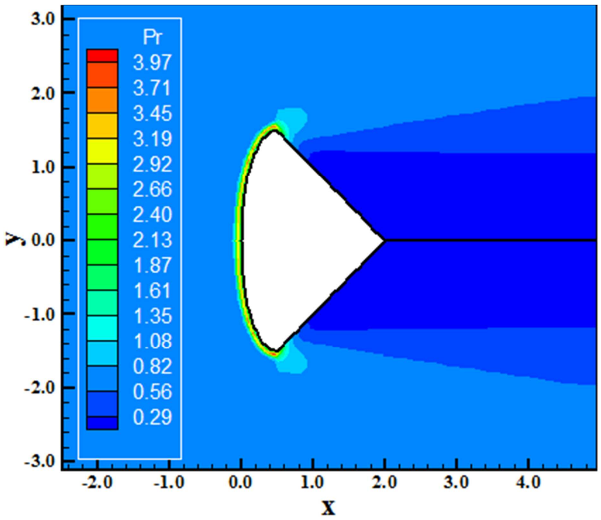

Figure 12. *Pressure contours (JK).*

Figure 14 presents the temperature contours obtained by the [2] scheme as using the [9] turbulence model. The temperature peak is under-predicted in relation to the [7] and [8] results. The flow is symmetrical, but is not developed. Figure 15 presents the turbulent kinetic energy contours obtained by the [2] scheme as using the [9] turbulence model. The maximum “k” appears at a short region near the trailing edge. The field is bad developed. It confirms the idea of the bad behavior of the k-ε model in the hypersonic regime.

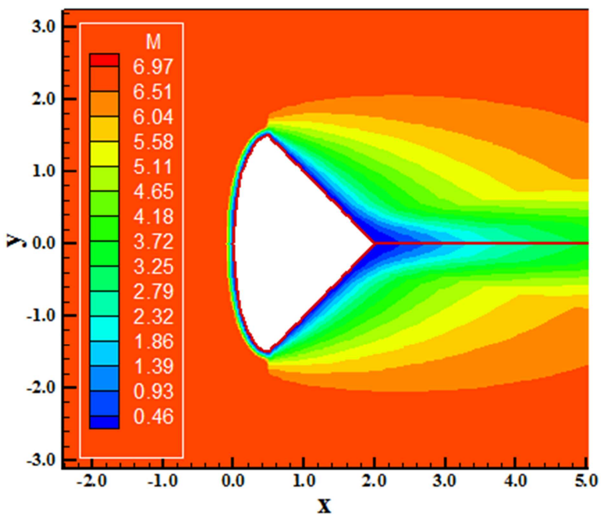

Figure 13. *Mach number contours (JK).*

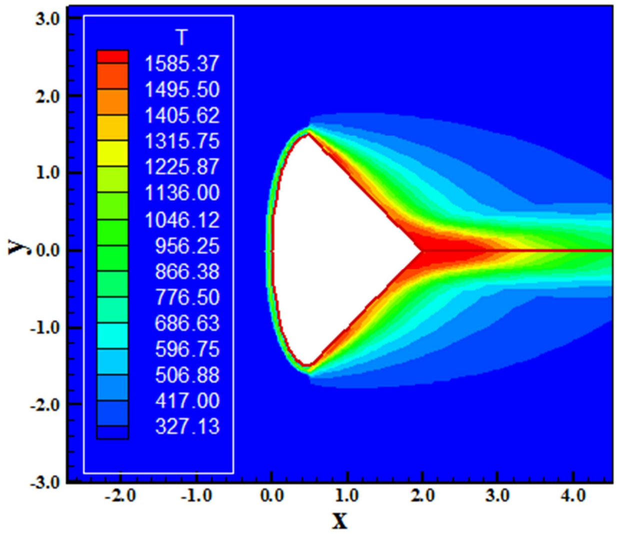

Figure 14. *Temperature contours (JK).*

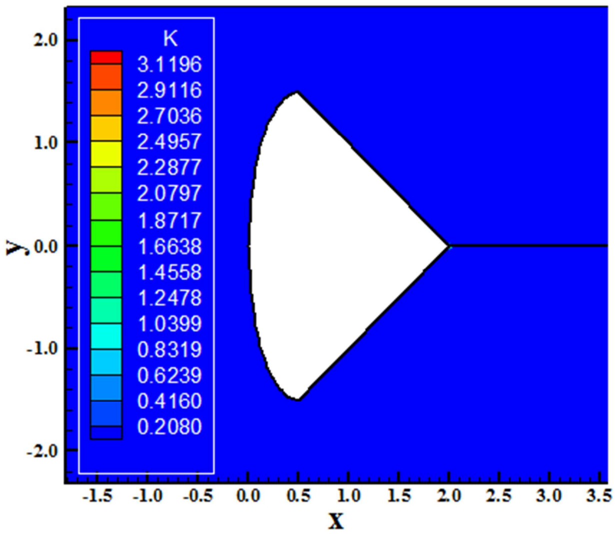

Figure 15. *Turbulent kinetic energy contours (JK).*

6.4. Zhou, Davidson and Olsson Results

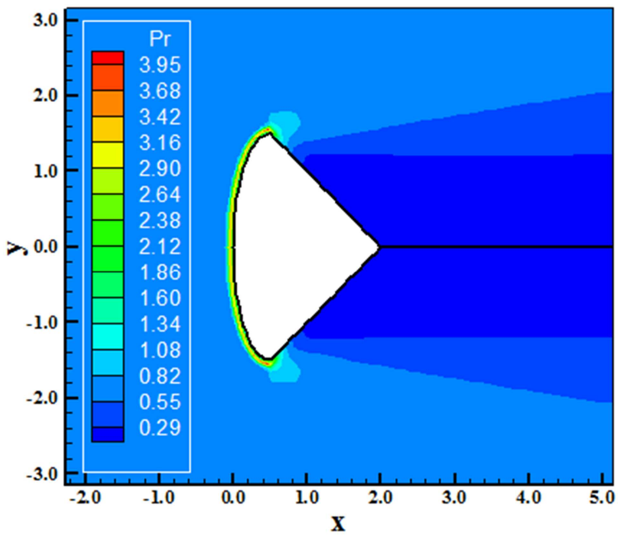

Figure 16. *Pressure contours (ZDO).*

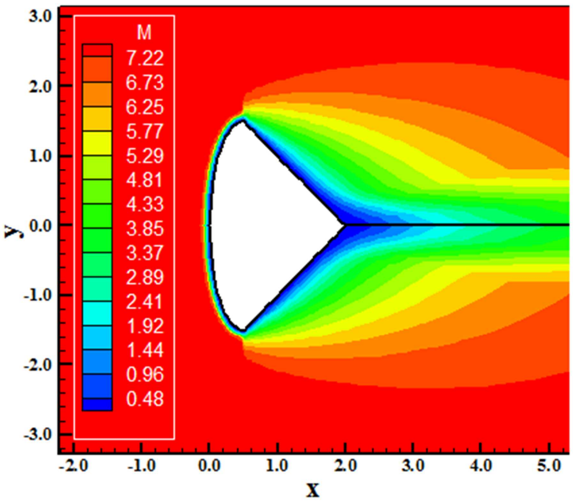

Figure 17. *Mach number contours (ZDO).*

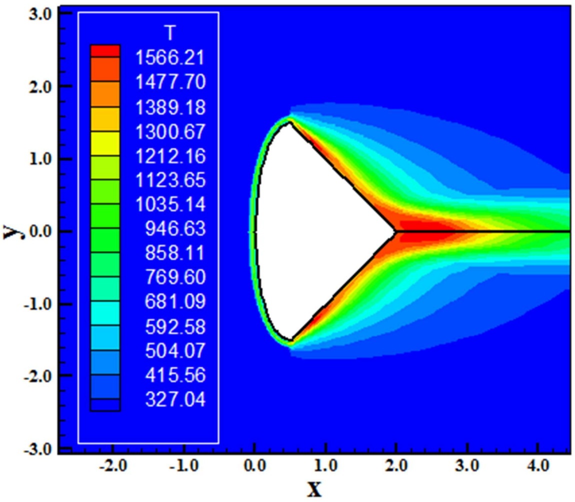

Figure 18. *Temperature contours (ZDO).*

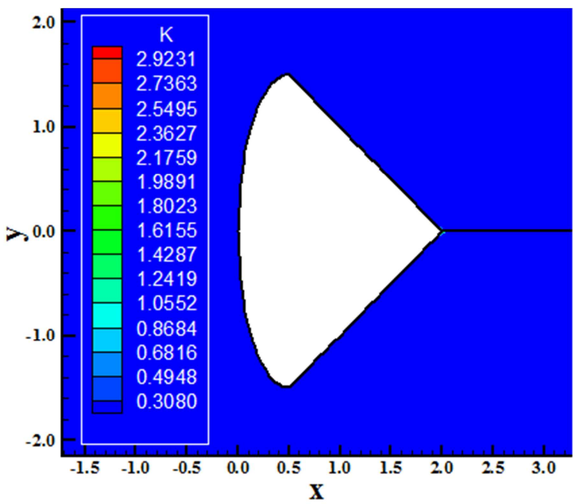

Figure 19. *Turbulent kinetic energy contours (ZDO).*

Figure 16 shows the pressure contours obtained by the [2] scheme as using the [10] turbulence model. The contours are symmetrical, but they seem not developed. The pressure peak is 3.95, distant from the results of [7] and [8]. Figure 17 shows the Mach number contours obtained by the [2] scheme as using the [10] turbulence model. Again, the contours seem not developed. The Mach number peak is 7.22, which is acceptable.

Figure 18 exhibits the temperature contours obtained by the [2] scheme as using the [10] turbulence model. The contours are symmetrical, but the temperature field is not developed. The maximum temperature is close to 1,566.21 K, distant from the respective maximum obtained by [7] and [8]. Figure 19 exhibits the turbulent kinetic energy contours. The maximum peak occurs at the trailing edge. The field is not developed.

6.5. –Cp Distributions

Figure 20 shows the –Cp distributions obtained by the [2] scheme as using the four turbulence models. As can be seen, the [9] and [10] distributions are wrong and confirm the idea of the bad response of the k-ε models to the hypersonic regime. [7] and [8] distributions are correct and are coincident, what indicate that the two solutions are very close.

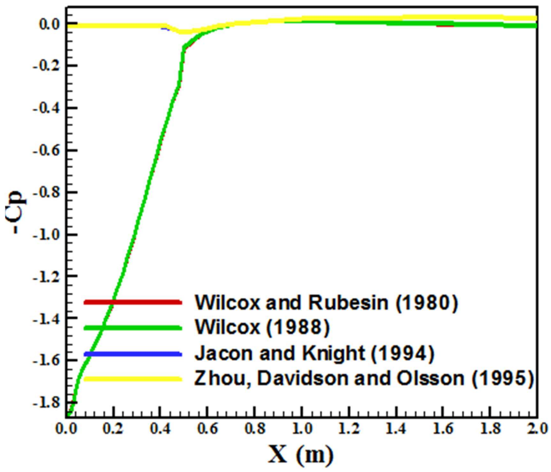

Figure 20. *–Cp distributions.*

6.6. Quantitative Analysis

Table 3 shows the lift and drag aerodynamic coefficients calculated by the [2] scheme in the turbulent cases. As the geometry is symmetrical and an attack angle of zero value was adopted in the simulations, the lift coefficient should have a zero value. The most correct value to the lift coefficient is due to the [7] turbulence model once that the [9] and [10] turbulence models present wrong solutions.

Table 3. *Aerodynamic coefficients of lift and drag.*

Turbulence Model:	c_L:	c_D:
[7] turbulence model	7.82×10^{-9}	2.27
[8] turbulence model	-2.32×10^{-8}	2.27
[9] turbulence model	1.73×10^{-7}	0.05
[10] turbulence model	-9.64×10^{-10}	0.05

Another possibility to quantitative comparison of the turbulent case is the determination of the stagnation pressure ahead of the configuration. [18] presents a table of normal shock wave properties in its B Appendix. This table permits the determination of some shock wave properties as function of the freestream Mach number. In front of the reentry capsule configuration, the shock wave presents a normal shock behavior, which permits the determination of the stagnation pressure, behind the shock wave, from the tables encountered in [18]. So it is possible to determine the ratio pr_0/pr_∞ from [18], where pr_0 is the stagnation pressure in front of the configuration and pr_∞ is the freestream pressure (equals to $1/\gamma$ to the present dimensionless).

Hence, to this problem, $M_\infty = 7.0$ corresponds to $pr_0/pr_\infty = 63.55$ and remembering that $pr_\infty = 0.714$, it is possible to conclude that $pr_0 = 45.37$. Values of the stagnation pressure to the turbulent cases and respective percentage errors are shown in Tab. 4. They are obtained from Figures 4, 8, 12, and 16. As can be observed, the [8] turbulence model has presented the best result, with a percentage error of 3.68%.

Table 4. *Values of the stagnation pressure and respective percentage errors.*

Turbulence Model:	pr_0:	Error (%):
[7] turbulence model	43.62	3.86
[8] turbulence model	43.70	3.68
[9] turbulence model	3.97	91.25
[10] turbulence model	3.95	91.29

Table 5. *Computational data.*

Turbulence Model:	CFL:	Iterations:
[7] turbulence model	0.10	11,124
[8] turbulence model	0.10	5,987
[9] turbulence model	0.10	1,052
[10] turbulence model	0.10	1,124

Finally, Table 5 exhibits the computational data of the present simulations. It can be noted that the most efficient scheme is the [2] one with the [8] turbulence model, considering that the [9] and [10] turbulence models have presented wrong solutions.

As final conclusion of this study, the [8] turbulence model was the best when comparing these four turbulence models: [7-10]. This choice is based on the second best estimative of the lift aerodynamic coefficient, considering the right results, and the best estimative to the stagnation pressure.

7. Conclusion

This work describes four turbulence models applied to hypersonic flows in two-dimensions. The [2] scheme, in its first-order version, is implemented to accomplish the numerical simulations. The Favre-averaged Navier-Stokes equations, on a finite volume context and employing structured spatial discretization, are applied to solve the "cold gas" hypersonic flow around a reentry capsule in two-dimensions. Turbulence models are applied to close the system, namely: [7-10]. The convergence process is accelerated to the steady state condition through a spatially variable time step procedure, which has proved effective gains in terms of computational acceleration (see [11-12]). The results have shown that the [7] scheme yields the best results in terms of the prediction of the lift aerodynamic coefficient; however, the [8] turbulence model predicts the best value of the stagnation pressure. Moreover, the [8] scheme also predicted the most severe pressure field. As final conclusion, the [8] turbulence model is the best in this work.

An important conclusion of this work was the deficiency of the k-ε models to simulate hypersonic flows. Good results of these models are obtained until the supersonic regime considering the first author's experience. Some results of the k-ε models to supersonic flows are detailed in [16-17; 19-20]. The reader is encouraged to read these references to see the positive features of these models.

Acknowledgment

The author would like also to thank the infrastructure of ITA that allowed the realization of this work.

References

[1] P. Kutler, "Computation of Three-Dimensional, Inviscid Supersonic Flows", Lecture Notes in Physics, Vol. 41, 1975, pp. 287-374.

[2] B. Van Leer, "Flux-Vector Splitting for the Euler Equations", Proceedings of the 8th International Conference on Numerical Methods in Fluid Dynamics, E. Krause, Editor, Lecture Notes in Physics, Vol. 170, 1982, pp. 507-512, Springer-Verlag, Berlin.

[3] R. Radespiel, and N. Kroll, "Accurate Flux Vector Splitting for Shocks and Shear Layers", Journal of Computational Physics, Vol. 121, 1995, pp. 66-78.

[4] M. Liou, and C. J. Steffen Jr., "A New Flux Splitting Scheme", Journal of Computational Physics, Vol. 107, 1993, pp. 23-39.

[5] T. Cebeci, and A. M. O. Smith, "A Finite-Difference Method for Calculating Compressible Laminar and Turbulent Boundary Layers", Journal of Basic Engineering, Trans. ASME. Series B. , Vol. 92, No. 3, 1970, pp. 523-535.

[6] B. S. Baldwin, and H. Lomax, "Thin Layer Approximation and Algebraic Model for Separated Turbulent Flows", AIAA Paper 78-257, 1978.

[7] D. C. Wilcox, and M. W. Rubesin, "Progress in Turbulence Modeling for Complex Flow Fields Including the Effects of Compressibility", NASA TP-1517, 1980.

[8] D. C. Wilcox, "Reassessment of the Scale-Determinig Equation for Advanced Turbulence Models", AIAA Journal, Vol. 26, 1988, pp. 1299-1310.

[9] F. Jacon, and D. Knight, "A Navier-Stokes Algorithm for Turbulent Flows Using an Unstructured Grid and Flux Difference Splitting", AIAA Paper 94-2292, 1994.

[10] G. Zhou, L. Davidson, and E. Olsson, "Turbulent Transonic Airfoil Flow Simulation Using a Pressure-Based Algorithm", AIAA Journal, Vol. 33, No. 1, 1995, pp. 42-47.

[11] E. S. G. Maciel, "Analysis of Convergence Acceleration Techniques Used in Unstructured Algorithms in the Solution of Aeronautical Problems – Part I", Proceedings of the XVIII International Congress of Mechanical Engineering (XVIII COBEM), 2005, Ouro Preto, MG, Brazil. [CD-ROM]

[12] E. S. G. Maciel, "Analysis of Convergence Acceleration Techniques Used in Unstructured Algorithms in the Solution of Aerospace Problems – Part II", Proceedings of the XII Brazilian Congress of Thermal Engineering and Sciences (XII ENCIT), 2008, Belo Horizonte. MG, Brazil. [CD-ROM]

[13] R. W. Fox, and A. T. McDonald, *Introdução à Mecânica dos Fluidos*, Ed. Guanabara Koogan, Rio de Janeiro, RJ, Brazil, 1988.

[14] L. N. Long, M. M. S. Khan, and H. T. Sharp, "Massively Parallel Three-Dimensional Euler/Navier-Stokes Method", AIAA Journal, Vol. 29, No. 5, 1991, pp. 657-666.

[15] D. J. Mavriplis, and A. Jameson, "Multigrid Solution of the Navier-Stokes Equations on Triangular Meshes", AIAA Journal, Vol. 28, No. 8, 1990, pp. 1415-1425.

[16] E. S. G. Maciel, "Assessment of Several Turbulence Models as Applied to Supersonic Flows in 2D – Part I", *Engineering and Technology*, Vol. 2, Issue 4, 2015, June, pp. 220-234.

[17] E. S. G. Maciel, "Assessment of Several Turbulence Models as Applied to Supersonic Flows in 2D – Part II", Submitted to *Engineering and Technology* (under review), 2015.

[18] J. D. Anderson Jr., *Fundamentals of Aerodynamics*, McGraw-Hill, Inc., EUA, 4^{th} Edition, 1008p, 2005.

[19] E. S. G. Maciel, "Assessment of Several Turbulence Models as Applied to Supersonic Flows in 2D – Part III", *Engineering and Technology*, Vol. 2, Issue 4, 2015, pp. 235-255.

[20] E. S. G. Maciel, "Assessment of Several Turbulence Models as Applied to Supersonic Flows in 2D – Part IV", Submitted to *Engineering and Technology* (under review), 2015.